Imaging, Diagnosis, Prognosis

Clinical Cancer Research

Combretastatin A-4 Phosphate Affects Tumor Vessel Volume and Size Distribution as Assessed Using MRI-Based Vessel Size Imaging

Thomas Nielsen[1,2,4], Lise Bentzen[1], Michael Pedersen[3], Trine Tramm[1], Paul F.J.W. Rijken[5], Johan Bussink[5], Michael R. Horsman[1], and Leif Østergaard[2]

Abstract

Purpose: Combretastatin A-4 disodium phosphate (CA4P) is a promising vascular disrupting agent (VDA) in clinical trials. As CA4P acts on dividing endothelial cells, we hypothesize that CA4P affects vessels of certain sizes. The aim of this study was to evaluate the effect of CA4P by the MRI-based vessel size imaging (VSI).

Experimental Design: C3H mammary carcinomas were grown to 200 mm^3 in the right rear foot of female CDF_1 mice. A control group of mice received no treatment, and a treatment group had CA4P administered intraperitoneally at a dose of 250 mg/kg. VSI was conducted on a 3 Tesla MR scanner to estimate the tumor blood volume (ζ_0) and mean vessel radius (R). Vascularization was also estimated histologically by endothelial and Hoechst 33342 staining.

Results: ζ_0 and R showed different spatial heterogeneity. Tumor median and quartile values of ζ_0 were all significantly reduced by about 35% in the CA4P-treated group as compared with the control group, and the median and upper quartile of R were significantly increased. Histograms of ζ_0 and R showed a general decrease in ζ_0 following treatment, and values of R in a certain range ($\approx$20–30 μm) were decreased in the treatment group. The drug-induced change in ζ_0 was in agreement with histology and our previous dynamic contrast enhanced MRI (DCE-MRI) data.

Conclusions: Tumor blood volume and mean vessel radius showed a clear response following treatment with CA4P. VSI may prove valuable in estimation of tumor angiogenesis and prediction of response to VDAs. *Clin Cancer Res; 18(23); 6469–77. ©2012 AACR.*

Introduction

Combretastatin A-4 disodium phosphate (CA4P) is a promising vascular disrupting agent (VDA) in clinical trials (1). It causes vascular damage and perfusion changes in different tumor types via cytotoxity and antiproliferative effects against mitotic endothelial cells, (2–6). Often, the largest effect is seen in the tumor center, because peripheral tumor cells form a viable rim (2, 3, 7), receiving nutrient supply from the vessels of adjacent normal tissue, which are unaffected by the treatment (8, 9). The mechanisms by which CA4P causes vascular shutdown, are complex and not completely understood (10). One interesting observation seen with intravital microscopy was that CA4P mainly decreased the number of small vessels (diameter < 10 μm; ref. 11). Further information on the vascular effects of the drug will improve the understanding of its mechanisms.

MRI offers a variety of methods to noninvasively estimate vascular characteristics—and thereby the action of CA4P. Dynamic contrast enhanced MRI (DCE-MRI) provides information about blood flow, vessel permeability, interstitial volume, and, depending on the choice of kinetic model, also blood plasma volume. It has been used in both experimental and clinical evaluation of tumor response to CA4P (12–17). Another approach is susceptibility-contrast MRI. Intravascular susceptibility contrast has been explored analytically, by simulations, and experimentally with the aim of understanding and using these effects in measurements of cerebral blood flow and blood volume and in functional MRI (18–23). A well-described difference in vessel size dependency of the gradient echo and spin echo signals—through the transverse relaxation rates R_2 and R_2^*—has led to the novel MRI method vessel size imaging (VSI; refs. 24–29). VSI quantitatively estimates blood volume and mean vessel size. The R_2^* relaxation rate difference

Authors' Affiliations: Departments of [1]Experimental Clinical Oncology; [2]Neuroradiology, Danish National Research Foundations Center of Functionally Integrative Neuroscience; [3]MR Research Center, Aarhus University Hospital; [4]Interdisciplinary Nanoscience Center, Aarhus University, Aarhus, Denmark; and [5]Department of Radiation Oncology, Radboud University Nijmegen Medical Centre, Nijmegen, The Netherlands

Corresponding Author: Thomas Nielsen, Department of Experimental Clinical Oncology, Aarhus University Hospital, Nørrebrogade 44, Building 5, DK-8000 Aarhus C, Denmark. Phone: 45-78463589; Fax: 45-86197109; E-mail: thomas@oncology.dk

doi: 10.1158/1078-0432.CCR-12-2014

Translational Relevance

In this study, the novel MRI method of vessel size imaging (VSI) was used for providing *in vivo* images of blood volume and mean vessel radius in untreated or combretastatin-treated C3H mammary carcinomas. The experiments were carried out on a 3 Tesla clinical MRI system using the intravascular contrast agent Sinerem, which belongs to a promising type of iron oxide contrast agents. The results show different blood volume and vessel radius distributions between treated tumors and controls, and they indicate that combretastatin acts on vessels of certain radii. These preclinical data suggest the role of VSI in planning and monitoring clinical treatments with combretastatin and other antivascular treatments, including optimization of combined treatments.

ΔR_2^* caused by an injected contrast agent is proportional to the blood volume independent of the vessel sizes from capillary and above, whereas ΔR_2 is most sensitive to vessels at capillary size. VSI can be conducted on cerebral dynamic susceptibility-contrast MRI data using standard gadolinium chelates (27), or iron oxide contrast agent (28), or in other organs using a contrast agent that remains intravascular for sufficient time to allow R_2 and R_2^* measurements at steady state (17, 24–26, 30–34).

We have recently evaluated the CA4P-induced vascular changes by DCE-MRI and susceptibility-contrast MRI (17, 35). The degree of vascular damage induced 3 hours after CA4P treatment was in agreement with the enhancement of radiation treatment when combined with CA4P. Previously, 2 to 4 hours was shown to be a good time point for monitoring the vascular effects of VDAs in preclinical studies (36, 37). We hypothesize that the proposed specificity of CA4P for vessels of particular sizes can be shown by VSI. The aim of this study was, therefore, to further characterize the effect of CA4P by VSI in this tumor model, in which we have previously characterized the effect of CA4P by DCE-MRI and other methods. VSI data on the tumor and treatment model used in our previous studies will greatly contribute to the overall knowledge about the tumor vasculature and its complex response to CA4P.

Materials and Methods

Animal and tumor model

C3H mammary carcinomas were implanted into the right rear foot of the female CDF_1 mice. The derivation and maintenance of this tumor have been described previously (38). Experiments were carried out when the tumors had reached approximately 200 mm^3 in size. Tumor volume was calculated from the formula $D1 \times D2 \times D3 \times \pi/6$, in which $D1$, $D2$, and $D3$ represent the 3 orthogonal diameters. The animals were divided into 2 groups; a control group, which received no treatment ($n = 21$), and a treatment group, which received CA4P treatment ($n = 22$). All experiments were carried out using nonanesthetized animals and were conducted under institutionally and nationally approved guidelines for animal welfare.

Drug preparation

CA4P (OXiGENE Inc.) was dissolved in saline immediately before each experiment and was kept cold and protected from light and given as a single intraperitoneal injection at a constant volume of 0.02 mL/g body weight at a dose of 250 mg/kg. Sinerem (Laboratoires Guerbet) was diluted in saline to the concentration 1.25 mg Fe/mL and was given intravenously at a dose of 2.5 mg Fe/kg body weight. Hoechst 33342 (Sigma Chemical Co.) was given intravenously at the dose 15 mg/kg.

MRI

MRI was carried out using a 3 Tesla system (Signa Excite HD, General Electric Medical Systems). CA4P-treated mice were scanned 3 hours after drug administration. Mice were restrained in specially constructed lucite jigs with the tumor-bearing leg exposed and loosely attached to the jig with tape without impairing the blood supply to the foot. The tail was restrained by tape, and a cannula connected via a 0.38-mm inner diameter line of 16-cm length to a syringe primed with contrast agent solution was applied intravenously in a tail vein. This line was primed with saline to prevent contrast agent from entering the circulation before injection. One or 2 mice were positioned in an upper extremity quadrature radiofrequency coil (Mayo Clinic BC-10 3.0 T, General Electric Medical Systems), and when 2 mice were positioned, their tumors were scanned simultaneously. When a single mouse was scanned, the image slice was positioned similarly through the tumor as for a scan of 2 mice.

R_2 and R_2^* measurements were conducted on a single oblique slice of 2-mm thickness before and immediately following contrast agent administration. Measurements were conducted using gradient echo and spin echo sequences with TR = 2,000 milliseconds, field of view = 4×4 cm, acquisition matrix 128×128 reconstructed to 256×256, and number of averages = 1. In the gradient echo sequence, the flip angle was 90°, and T_E was 6, 10, 20, and 30 milliseconds. The spin echo T_E was 15, 30, 40, 45, 60, 80, 120, and 160 milliseconds. For both sequences, the echoes were obtained in 2 excitations. The total scan time following contrast agent administration (17 minutes) was kept within the time interval of constant blood concentration of contrast agent, which was previously estimated by dynamic R_2 and R_2^* measurements in 2 separate untreated test tumors, respectively. Following contrast agent administration, R_2 and R_2^* remained significantly decreased (one-sample t test on differences) during the 60 minutes of this test (results not shown). Six mice from each treatment group were subject to the histologic analysis described later, the others were euthanized by cervical dislocation after MRI.

MRI data analysis

Analysis was conducted using MATLAB 7.12 (The MathWorks, Inc.). R_2 and R_2^* maps were produced by nonlinear

least squares fitting of the image signal S to the equation $S(T_E) = S(0) \cdot e^{-T_E \cdot R_2^*}$ following image smoothing by convolution with a Gaussian kernel of 5 voxels in size and a SD of 1. $\Delta R_2^{(*)}$ maps were produced by subtracting precontrast maps from corresponding postcontrast maps. Regions of interest (ROI) were defined on the basis of a T_2-weighted image, and ROI voxels were excluded from the analysis if they displayed unphysiologic values (i.e., $\Delta R_2 \leq 0$, $\Delta R_2^* \leq 0$, or $\Delta R_2^* \leq \Delta R_2$) due to noise.

The blood fraction, ζ_0, and the vessel size index, R (mean vessel size), were then calculated voxelwise by the equations (25):

$$\zeta_0 = \frac{3}{4\pi} \frac{\Delta R_2^*}{\gamma \Delta \chi B_0} \quad (1)$$

$$R = 0.424 \left(\frac{D}{\gamma \Delta \chi B_0} \right)^{\frac{1}{2}} \left(\frac{\Delta R_2^*}{\Delta R_2} \right)^{\frac{3}{2}} \quad (2)$$

where γ is the gyromagnetic ratio, $\Delta\chi$ is the magnetic susceptibility difference between the intra- and extravascular compartments (in cgs units), B_0 is the applied magnetic field strength, and D is the diffusion coefficient. $\Delta\chi$ was interpolated from ref. (26) to 0.128 ppm, and D was assumed to be 0.5×10^{-9} m^2/s based on measurements on the C3H tumor (39). Quartiles of the parameter values were calculated from each tumor for comparison by Student t test with $P < 0.05$ considered statistically significant. All tumor voxels in each group were pooled to obtain common parameter histograms for each treatment group.

Histology

Following MRI, the functional perfusion marker Hoechst 33342 was injected intravenously through the line into the tail vein of the mice subject to histology. After 1-minute circulation time, the mice were euthanized by cervical dislocation. The tumors were excised and snap frozen. A 6-μm frozen section of the central part of each tumor was cut in a cryostat at −20°C and mounted to a glass slide.

Semiquantitative fluorescence microscopy analysis of the tumor sections was conducted for deriving vascular information from the fluorescent perfusion marker Hoechst 33342 and immunofluorescent histologic detection of the endothelial marker 9F1 [a rat monoclonal antibody to mouse endothelium; Radboud University Nijmegen Medical Centre (Nijmegen, The Netherlands)]. The procedure is previously described by Rijken and colleagues and Hendriksen and colleagues (40, 41). The following parameters were estimated: relative vascular area, relative perfused tumor area, perfused fraction, number of vascular structures, vessel density, number of perfused vascular structures, perfused vessel density, number fraction of perfused vessels, mean vessel size, and mean perfused vessel size. In short, perfused vascular structures were represented by the result of the logical "AND" operation on the images with the vascular structures (9F1) and the perfused areas (Hoechst 33342). In our data, vessels can have more than 1 perfused area around itself, alternating with nonperfused areas. This leads to an overestimation of the number of perfused vascular structures for this vessel. To correct for this, these perfused vascular structures—belonging to the same vessel—were considered as 1 perfused vascular structure. This was done by image processing using conditional dilation of the image with the perfused vascular structures, resulting in vascular structures that were completely perfused. Student t test was used for comparison with $P < 0.05$ considered statistically significant.

Results

Figure 1 shows a typical example of vessel maps for an untreated tumor. The blood volume (ζ_0) maps showed heterogeneity across the tumor with areas of high blood volume typically in peripheral regions rather than in the tumor center. Maps of mean vessel radius R also showed heterogeneity and indicated that areas of high blood volume and large vessels do not always colocalize. In Fig. 2 are the parameters ζ_0, ΔR_2, and R shown as mean (±1 SEM) of individual tumor quartiles. The total blood volume ζ_0 is a scaling of ΔR_2^*, whereas ΔR_2 is proportional to microvascular blood volume. CA4P significantly decreased all 3 quartiles of ζ_0 ($P < 10^{-7}$) and ΔR_2 ($P < 10^{-4}$) indicating a general reduction in vascular volume. The drug increased the median and upper quartile values of R, although not significantly, indicating a complex change in the distribution of R. The small SEs showed uniformity across individual tumors, and

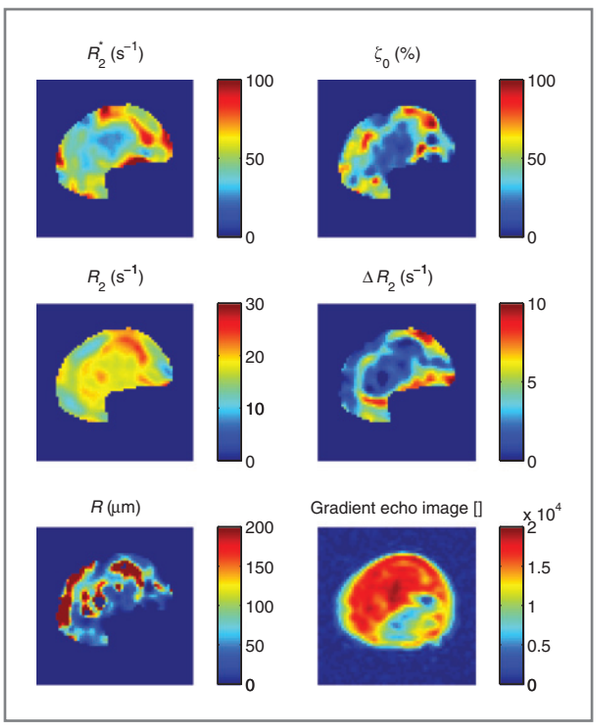

Figure 1. Parametric maps for an untreated tumor showing heterogeneity in all parameters and a gradient echo image ($T_E = 6$ milliseconds) showing the foot containing the tumor.

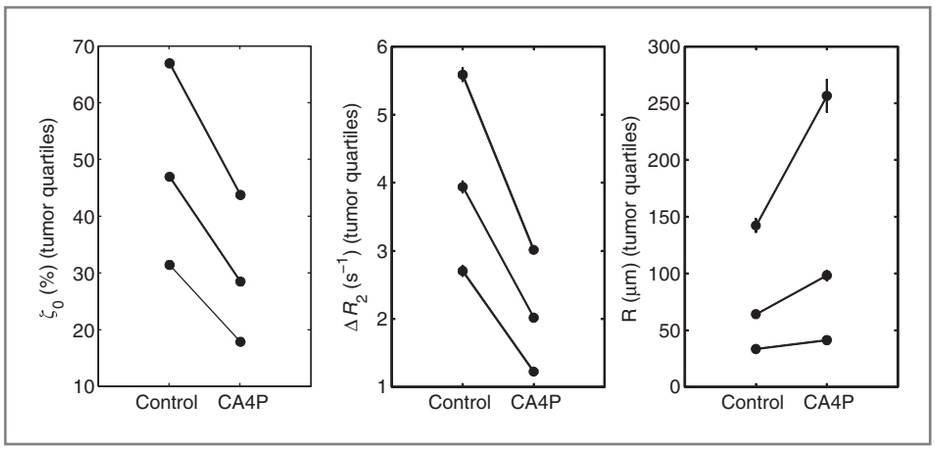

Figure 2. Tumor quartile values (mean ± 1 SEM) of the parameters (from left) blood volume ζ_0, ΔR_2 (proportional to microvascular blood volume), and mean vessel radius *R*.

voxel data were therefore pooled across tumors in subsequent analysis.

The common histograms of ζ_0 for both groups are shown in Fig. 3A. The distribution was shifted toward lower values as indicated by individual quartiles in Fig. 2. Corresponding histograms of *R* are shown in Fig. 3B. They showed that for CA4P-treated tumors, values of *R* in a certain vessel radius range (≈20–30 μm) were decreased as compared with untreated tumors.

Figure 4A shows histograms of R_2 values obtained before administration of contrast agent. This parameter depends inversely on the amount of free water in, for example, inflammatory tissue. Compared with untreated tumors, the R_2 values of the CA4P-treated tumors were shifted toward higher values with a slightly different distribution shape. The quartiles were all significantly increased ($P < 10^{-4}$). This may indicate a reduction in extracellular water diffusion due to cell swelling as a consequence of CA4P-induced hypoxia. In Fig. 4B are shown corresponding histograms for ΔR_2^*, which has been related to blood deoxyhemoglobin (42–44). CA4P changed the distribution shape toward higher values indicating lower blood oxygenation. The quartiles were all significantly increased ($P < 0.05$).

Combined images of 9F1 and Hoechst 33342 for a control tumor and a treated tumor are shown in Fig. 5. They visualize the lower amount of functional vessels following CA4P treatment. The histologically estimated parameters are summarized in Table 1. The perfused fraction of the vascularized tumor area, number fraction of perfused vessels, relative perfused tumor area, and perfused vessels density, were significantly lower in the CA4P-treated group. Neither of the estimates of mean vessel size showed statistical significance.

Discussion

Our results confirm the vascular targeting properties of CA4P in the C3H mammary carcinoma and further suggest that the drug selectively reduces the proportion of vessels with radii in the range (≈20–30 μm) in this tumor type. Bearing in mind that CA4P acts specifically on dividing endothelial cells (2), our results may be explained by different mitotic activities in vessels of different calibers. The results are in agreement with those obtained by Walker-Samuel and colleagues in an orthotopic murine PC3 prostate tumor xenograft 24 hours following treatment with ZD6126, another tubulin-binding agent (45). Using VSI, they found similar treatment-induced reductions in blood volume, relaxation rates R_2 and R_2^*, and mean vessel diameter *R*. The pre- and posttreatment histogram shapes of *R* are in qualitative agreement with those obtained in our study supporting a common mechanism of action for the 2 tubulin-binding agents. The peak in the histogram for pretreatment *R* occurs at a slightly higher vessel size in our study, which may be attributed to scaling problems as addressed later, and while the increases in median and upper quartile of *R* in our study were not significant, they found significant reductions in percentiles at 60% and below. Our finding is also in agreement with intravital microscopy data on CA4P activity showing that reduction in venule number is largest for small venules (diameter < 10 μm), and that reduction in arteriolar diameter occurs (11). The distribution of *R* in the current study may reflect the combination of these vascular effects. The reduction in vessels with radii in the interval (≈20–30 μm) could reflect the reported reduction in small venules. As the number of vessels with radii less than 20 μm increased, reduction in vessel diameter could also contribute to the *R* histogram shape change. The vessel size distribution change did not significantly change the quartiles of *R* or the histologic mean vessel size estimates. The drug-induced change in ζ_0 was confirmed by significant reductions in histologic parameters reflecting perfused vessels. It is also in qualitative agreement with our susceptibility imaging (similar blood volume estimates) and DCE-MRI results on the same tumor model (17, 35) and further improved our knowledge about tumor vascular responses to CA4P by providing information on which vessel calibers are targeted by the treatment.

Our study has a number of potential shortcomings. The comparison of individual tumor parameter quartiles (Fig. 2) showed excellent agreement between individual tumor parameter value distributions. Evaluation of the drug effects

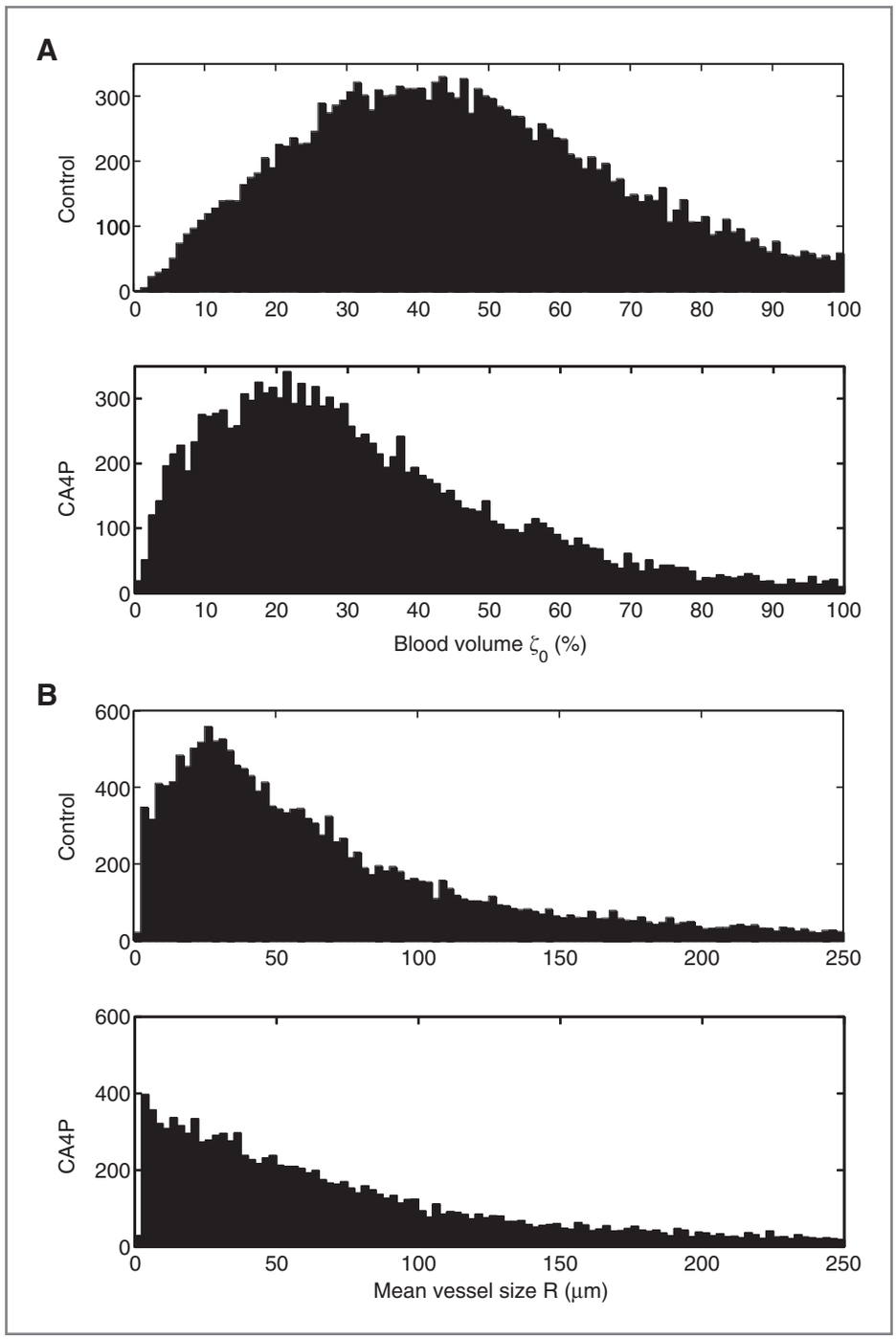

Figure 3. Histograms showing the distribution of pooled (A) ζ_0 voxel values for the 2 treatment groups and (B) *R* voxel values for the 2 treatment groups.

were, therefore, conducted from pooled histograms. This approach may, however, not necessarily apply in more heterogeneous tumor models or tumor types. Only 1 model was actually used in this study and that was our C3H mammary carcinoma. We focused on this model because our previous studies using DCE-MRI to monitor vascular changes after treatment with CA4P have shown effects in this tumor model that were identical to those recorded in patients with a variety of tumor types using equivalent drug doses (35).

Absolute values of ζ_0 are relatively large and may be overestimated; previous estimates of vascular volume in the C3H mammary carcinoma about 200 μm are about 18% (46, 47). Theoretical reasons may include that equations (1) and (2) are valid for small blood fractions and high $\Delta\chi$ only (18, 25). We chose a clinically relevant dose of contrast

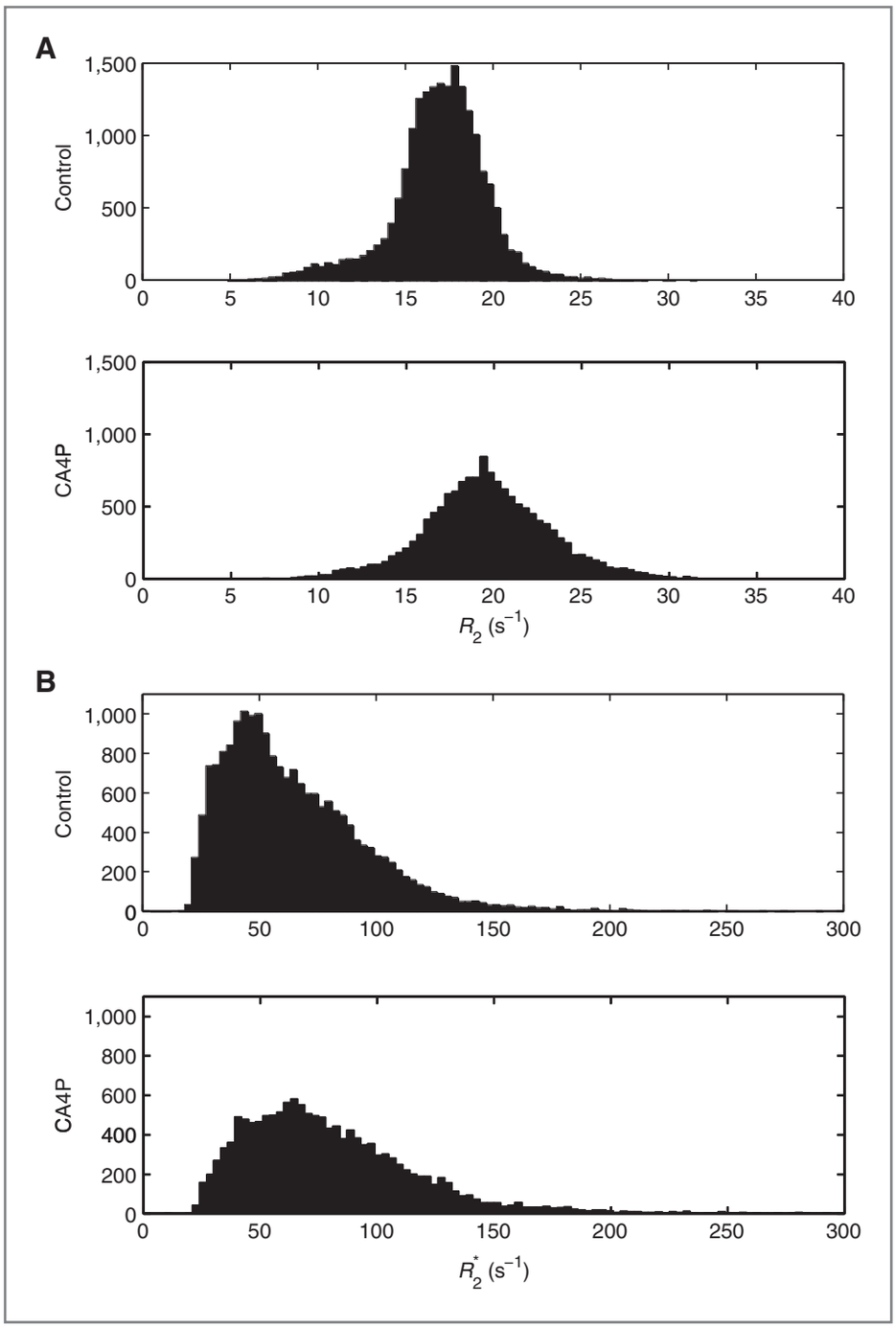

Figure 4. Histograms showing the distribution of pooled (A) initial R_2 voxel values for the 2 treatment groups and (B) initial R_2^* voxel values for the 2 treatment groups.

agent, and doses in this range have been shown to overestimate R (26). Other sources of scaling errors may be the assumptions of $\Delta\chi$ (for estimation of both ζ_0 and R) and D (for estimation of R). The adoption of $\Delta\chi$ estimated in rats for mice may cause a scaling error because of different blood volumes relative to weight, but this would be small between these species. The overall qualitative evaluation of the drug effect was, however, independent of a systematic scaling.

The change in R_2 following CA4P treatment depended critically on the diffusion coefficient, D. The drug action may induce changes in cellularity that subsequently affects D. Therefore, diffusion changes in the tumor tissue could affect the comparison of R between the treatment groups. Most probably, cells in the CA4P-treated tumors would swell because of hypoxia following vascular shutdown. This would increase the extracellular diffusion, which to a high degree determines D, and consequently R would be

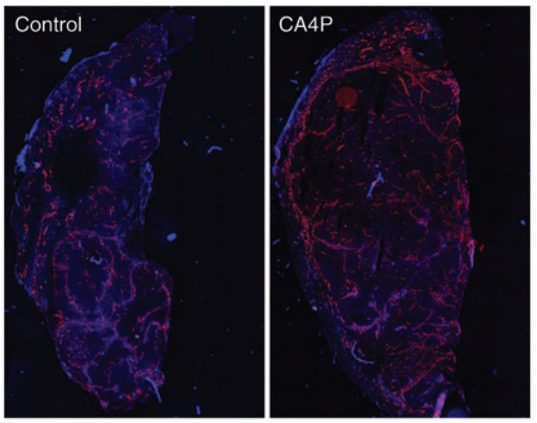

Figure 5. Combined images of endothelial staining (9F1), red, and perfusion staining (Hoechst 33342), blue. The left tumor section is from a control tumor, and the right tumor section is from a CA4P treated tumor.

underestimated in the CA4P-treated group. Furthermore, D may be heterogeneous across tumors in both treatment groups. These effects suggest that maps of D should be measured in the individual tumors.

CA4P changed the R_2^* distribution shape toward higher values indicating lower blood oxygenation 3 hours following VDA treatment. Recent studies in the rat GH3 prolactinoma have shown an R_2^* increase 35 minutes following VDA treatment (48, 49), but this was not the case for CA4P (49). Twenty-four hours following treatment with CA4P and other VDAs, R_2^* decreased. The interpretation of R_2^* is complex as both the initial increase and the following decrease are related to perfusion changes; the initial increase is related to larger deoxyhemoglobin levels, and the following decrease related to reduced blood volume. R was distributed differently between the treatment groups showing that certain vessel calibers were affected by CA4P. It should be further investigated whether the distribution of R provides information of angiogenic status or predicts response to VDAs or other treatments.

Table 1. Histologic vascular parameters for the 2 treatment groups

Parameter Mean ± 1 SE	Control group $n = 6$	CA4P group $n = 6$
Perfused fraction	0.83 ± 0.02	0.52 ± 0.08[a]
Relative vascular area	0.069 ± 0.010	0.050 ± 0.008
Relative perfused tumor area	0.058 ± 0.010	0.026 ± 0.005[a]
Vascular density	159 ± 8	155 ± 12
Perfused vessel density	123 ± 8	76 ± 8[a]
Number of vascular structures	3,347 ± 673	3,338 ± 481
Number of perfused vascular structures	2,603 ± 536	1,754 ± 413
Number fraction of perfused vessels	0.78 ± 0.02	0.51 ± 0.06[a]
Mean vessel size, μm^2	440 ± 67	318 ± 30
Mean perfused vessel size, μm^2	477 ± 81	325 ± 38

NOTE: Results show mean ± 1 SEM.
[a]Parameters significantly different between the groups.

Despite numerous favorable scientific results being obtained using Sinerem, the clinical development of this agent has now been halted. Other ultrasmall superparamagnetic iron oxide (USPIO) agents have suffered similar fates in the past, but the development of new nanoparticle formulations provide hope that clinically available iron-containing particles can be introduced into the clinic; many of these exhibit prolonged plasma half life, particularly useful for angiographic purposes, or for monitoring antiangiogenic treament. One example is the U.S. Food and Drug Administration (FDA)-approved USPIO compound ferumoxytol (Feraheme, AMAG Pharmaceuticals Inc.) that has recently been shown as a biomarker to identify tumor-associated macrophages (50).

Conclusions

Estimates of blood fraction and mean vessel size showed a clear response of the tumor model to CA4P. The large change in blood volume is in agreement with histology and our DCE-MRI results on the same tumor model, and the change in distribution of mean vessel size agrees with a study using a different assay. This may be a consequence of different mitotic activity in vessels of different calibers as CA4P acts on dividing endothelial cells only. VSI may be valuable in assessing tumor angiogenesis and prediction of response to VDAs.

Disclosure of Potential Conflicts of Interest

M.R. Horsman is a consultant for OXiGENE. No potential conflicts of interest were disclosed by the other authors.

Authors' Contributions

Conception and design: T. Nielsen, L. Bentzen, L. Østergaard
Development of methodology: T. Nielsen, L. Bentzen, L. Østergaard
Acquisition of data (provided animals, acquired and managed patients, provided facilities, etc.): T. Nielsen, L. Bentzen, T. Tramm, J. Bussink
Analysis and interpretation of data (e.g., statistical analysis, biostatistics, computational analysis): T. Nielsen, L. Bentzen, P.F.J.W. Rijken, J. Bussink, L. Østergaard
Writing, review, and/or revision of the manuscript: T. Nielsen, L. Bentzen, M. Pedersen, T. Tramm, J. Bussink, M.R. Horsman, L. Østergaard
Administrative, technical, or material support (i.e., reporting or organizing data, constructing databases): T. Nielsen
Study supervision: L. Bentzen, M. Pedersen, M.R. Horsman, L. Østergaard

Acknowledgments

The authors thank Ms. Inger Marie Horsman, Dorthe Grand, Pia Schjerbeck, and Marianne Verner Bjerre for excellent technical assistance with the animals; Mogens J. Johannsen and Johannes P.W. Peters for excellent histologic work and analysis; OXiGENE for supplying CA4P; and Laboratoires Guerbet for supplying Sinerem.

Grant Support

This study is supported by The Danish Cancer Society, the Danish Council for Independent Research: Medical Sciences, the Danish National Research Foundation, Danish Programme Commission on Strategic Growth

Technologies (NaBIIT) grant nr. 2106-05-0031, and CIRRO—The Lundbeck Foundation Center for Interventional Research in Radiation Oncology and The Danish Council for Strategic Research.

The costs of publication of this article were defrayed in part by the payment of page charges. This article must therefore be hereby marked *advertisement* in accordance with 18 U.S.C. Section 1734 solely to indicate this fact.

Received June 19, 2012; revised September 17, 2012; accepted October 2, 2012; published OnlineFirst October 15, 2012.

References

1. Siemann DW, Chaplin DJ, Walicke PA. A review and update of the current status of the vasculature-disabling agent combretastatin-A4 phosphate (CA4P). Expert Opin Investig Drugs 2009;18:189–97.
2. Dark GG, Hill SA, Prise VE, Tozer GM, Pettit GR, Chaplin DJ. Combretastatin A-4, an agent that displays potent and selective toxicity toward tumor vasculature. Cancer Res 1997;57:1829–34.
3. Li L, Rojiani A, Siemann DW. Targeting the tumor vasculature with combretastatin A-4 disodium phosphate: effects on radiation therapy. Int J Radiat Oncol Biol Phys 1998;42:899–903.
4. Tozer GM, Prise VE, Wilson J, Locke RJ, Vojnovic B, Stratford MR, et al. Combretastatin A-4 phosphate as a tumor vascular-targeting agent: early effects in tumors and normal tissues. Cancer Res 1999;59:1626–34.
5. Murata R, Overgaard J, Horsman MR. Comparative effects of combretastatin A-4 disodium phosphate and 5,6-dimethylxanthenone-4-acetic acid on blood perfusion in a murine tumour and normal tissues. Int J Radiat Biol 2001;77:195–204.
6. Siemann DW, Mercer E, Lepler S, Rojiani AM. Vascular targeting agents enhance chemotherapeutic agent activities in solid tumor therapy. Int J Cancer 2002;99:1–6.
7. Grosios K, Holwell SE, McGown AT, Pettit GR, Bibby MC. *In vivo* and *in vitro* evaluation of combretastatin A-4 and its sodium phosphate prodrug. Br J Cancer 1999;81:1318–27.
8. Chaplin DJ, Pettit GR, Hill SA. Anti-vascular approaches to solid tumour therapy: evaluation of combretastatin A4 phosphate. Anticancer Res 1999;19:189–95.
9. Siemann DW. Vascular targeting agents. Horizons Cancer Ther 2002;3:4–15.
10. Tozer GM, Kanthou C, Baguley BC. Disrupting tumour blood vessels. Nat Rev Cancer 2005;5:423–35.
11. Tozer GM, Prise VE, Wilson J, Cemazar M, Shan S, Dewhirst MW, et al. Mechanisms associated with tumor vascular shut-down induced by combretastatin A-4 phosphate: intravital microscopy and measurement of vascular permeability. Cancer Res 2001;61:6413–22.
12. Dowlati A, Robertson K, Cooney M, Petros WP, Stratford M, Jesberger J, et al. A phase I pharmacokinetic and translational study of the novel vascular targeting agent combretastatin a-4 phosphate on a single-dose intravenous schedule in patients with advanced cancer. Cancer Res 2002;62:3408–16.
13. Galbraith SM, Maxwell RJ, Lodge MA, Tozer GM, Wilson J, Taylor NJ, et al. Combretastatin A4 phosphate has tumor antivascular activity in rat and man as demonstrated by dynamic magnetic resonance imaging. J Clin Oncol 2003;21:2831–42.
14. Stevenson JP, Rosen M, Sun W, Gallagher M, Haller DG, Vaughn D, et al. Phase I trial of the antivascular agent combretastatin A4 phosphate on a 5-day schedule to patients with cancer: magnetic resonance imaging evidence for altered tumor blood flow. J Clin Oncol 2003;21:4428–38.
15. Beauregard DA, Hill SA, Chaplin DJ, Brindle KM. The susceptibility of tumors to the antivascular drug combretastatin A4 phosphate correlates with vascular permeability. Cancer Res 2001;61:6811–5.
16. Maxwell RJ, Wilson J, Prise VE, Vojnovic B, Rustin GJ, Lodge MA, et al. Evaluation of the anti-vascular effects of combretastatin in rodent tumours by dynamic contrast enhanced MRI. NMR Biomed 2002;15:89–98.
17. Bentzen L, Vestergaard-Poulsen P, Nielsen T, Overgaard J, Bjørnerud A, Briley-Saebø K, et al. Intravascular contrast agent-enhanced MRI measuring contrast clearance and tumor blood volume and the effects of vascular modifiers in an experimental tumor. Int J Radiat Oncol Biol Phys 2005;61:1208–15.
18. Yablonskiy DA, Haacke EM. Theory of NMR signal behavior in magnetically inhomogeneous tissues: the static dephasing regime. Magn Reson Med 1994;32:749–63.
19. Kennan RP, Zhong J, Gore JC. Intravascular susceptibility contrast mechanisms in tissues. Magn Reson Med 1994;31:9–21.
20. Boxerman JL, Hamberg LM, Rosen BR, Weisskoff RM. MR contrast due to intravascular magnetic susceptibility perturbations. Magn Reson Med 1995;34:555–66.
21. Østergaard L, Weisskoff RM, Chesler DA, Gyldensted C, Rosen BR. High resolution measurement of cerebral blood flow using intravascular tracer bolus passages. part I: mathematical approach and statistical analysis. Magn Reson Med 1996;36:715–25.
22. Østergaard L, Sørensen AG, Kwong KK, Weisskoff RM, Gyldensted C, Rosen BR. High resolution measurement of cerebral blood flow using intravascular tracer bolus passages. part II: experimental comparison and preliminary results. Magn Reson Med 1996;36:726–36.
23. Kiselev VG. On the theoretical basis of perfusion measurements by dynamic susceptibility contrast MRI. Magn Reson Med 2001;46:1113–22.
24. Dennie J, Mandeville JB, Boxerman JL, Packard SD, Rosen BR, Weisskoff RM. NMR imaging of changes in vascular morphology due to tumor angiogenesis. Magn Reson Med 1998;40:793–9.
25. Troprès I, Grimault S, Vaeth A, Grillon E, Julien C, Payen JF, et al. Vessel size imaging. Magn Reson Med 2001;45:397–408.
26. Troprès I, Lamalle L, Farion R, Segebarth C, Rémy C. Vessel size imaging using low intravascular contrast agent concentrations. MAGMA 2004;17:313–6.
27. Kiselev VG, Strecker R, Ziyeh S, Speck O, Hennig J. Vessel size imaging in humans. Magn Reson Med 2005;53:553–63.
28. Quarles CC, Schmainda KM. Assessment of the morphological and functional effects of the anti-angiogenic agent SU11657 on 9L gliosarcoma vasculature using dynamic susceptibility contrast MRI. Magn Reson Med 2007;57:680–7.
29. Lemasson B, Valable S, Farion R, Krainik A, Remy C, Barbier EL. *In vivo* imaging of vessel diameter, size, and density: a comparative study between MRI and histology. Magn Reson Med. 2012 Mar 16. [Epub ahead of print].
30. Robinson SP, Rijken PF, Howe FA, McSheehy PM, van der Sanden BP, Heerschap A, et al. Tumor vascular architecture and function evaluated by non-invasive susceptibility MRI methods and immunohistochemistry. J Magn Reson Imaging 2003;17:445–54.
31. Kostourou V, Robinson SP, Whitley GS, Griffiths JR. Effects of overexpression of dimethylarginine dimethylaminohydrolase on tumor angiogenesis assessed by susceptibility magnetic resonance imaging. Cancer Res 2003;63:4960–6.
32. Robinson SP, Howe FA, Griffiths JR, Ryan AJ, Waterton JC. Susceptibility contrast magnetic resonance imaging determination of fractional tumor blood volume: a noninvasive imaging biomarker of response to the vascular disrupting agent ZD6126. Int J Radiat Oncol Biol Phys 2007;69:872–9.
33. Robinson SP, Ludwig C, Paulsson J, Ostman A. The effects of tumor-derived platelet-derived growth factor on vascular morphology and function *in vivo* revealed by susceptibility MRI. Int J Cancer 2008;122:1548–56.
34. Howe FA, McPhail LD, Griffiths JR, McIntyre DJ, Robinson SP. Vessel size index magnetic resonance imaging to monitor the effect of antivascular treatment in a rodent tumor model. Int J Radiat Oncol Biol Phys 2008;71:1470–6.
35. Nielsen T, Murata R, Maxwell RJ, Stødkilde-Jørgensen H, Ostergaard L, Horsman MR. Preclinical studies to predict efficacy of vascular

changes induced by combretastatin a-4 disodium phosphate in patients. Int J Radiat Oncol Biol Phys 2008;70:859–66.
36. Murata R, Overgaard J, Horsman MR. Potentiation of the anti-tumour effect of hyperthermia by combining with the vascular targeting agent 5,6-dimethylxanthenone-4-acetic acid. Int J Hyperthermia 2001;17: 508–19.
37. Horsman MR, Murata R. Vascular targeting effects of ZD6126 in a C3H mouse mammary carcinoma and the enhancement of radiation response. Int J Radiat Oncol Biol Phys 2003;57:1047–55.
38. Overgaard J. Simultaneous and sequential hyperthermia and radiation treatment of an experimental tumor and its surrounding normal tissue *in vivo*. Int J Radiat Oncol Biol Phys 1980;6:1507–17.
39. Chen G, Jespersen S, Pedersen M, Pang Q, Horsman MR, Jørgensen HS. Evaluation of anti-vascular therapy with texture analysis. Anticancer Res 2005;25:3399–405.
40. Rijken PF, Bernsen HJ, van der Kogel AJ. Application of an image analysis system to the quantitation of tumor perfusion and vascularity in human glioma xenografts. Microvasc Res 1995;50: 141–53.
41. Hendriksen EM, Span PN, Schuuring J, Peters JP, Sweep FC, van der Kogel AJ, et al. Angiogenesis, hypoxia and VEGF expression during tumour growth in a human xenograft tumour model. Microvasc Res 2009;77:96–103.
42. Abramovitch R, Dafni H, Smouha E, Benjamin LE, Neeman M. *In vivo* prediction of vascular susceptibility to vascular susceptibility endothelial growth factor withdrawal: magnetic resonance imaging of C6 rat glioma in nude mice. Cancer Res 1999;59:5012–6.
43. Kostourou V, Robinson SP, Cartwright JE, Whitley GS. Dimethylarginine dimethylaminohydrolase I enhances tumour growth and angiogenesis. Br J Cancer 2002;87:673–80.
44. Robinson SP, McIntyre DJ, Checkley D, Tessier JJ, Howe FA, Griffiths JR, et al. Tumour dose response to the antivascular agent ZD6126 assessed by magnetic resonance imaging. Br J Cancer 2003;88: 1592–7.
45. Walker-Samuel S, Boult JK, McPhail LD, Box G, Eccles SA, Robinson SP. Non-invasive *in vivo* imaging of vessel calibre in orthotopic prostate tumour xenografts. Int J Cancer 2012;130:1284–93.
46. Hilmas DE, Gillette EL. Morphometric analyses of the microvasculature of tumors during growth and after x-irradiation. Cancer 1974;33: 103–10.
47. Hilmas DE, Gillette EL. Microvasculature of C3H/Bi mouse mammary tumors after x-irradiation. Radiat Res 1975;61:128–43.
48. Robinson SP, Kalber TL, Howe FA, McIntyre DJ, Griffiths JR, Blakey DC, et al. Acute tumor response to ZD6126 assessed by intrinsic susceptibility magnetic resonance imaging. Neoplasia 2005;7:466–74.
49. McPhail LD, Griffiths JR, Robinson SP. Assessment of tumor response to the vascular disrupting agents 5,6-dimethylxanthenone-4-acetic acid or combretastatin-A4-phosphate by intrinsic susceptibility magnetic resonance imaging. Int J Radiat Oncol Biol Phys 2007;69: 1238–45.
50. Daldrup-Link HE, Golovko D, Ruffell B, Denardo DG, Castaneda R, Ansari C, et al. MRI of tumor-associated macrophages with clinically applicable iron oxide nanoparticles. Clin Cancer Res 2011;17: 5695–704.